

Spin dynamics and coherent tunnelling in the molecular magnetic rings Fe_6 and Fe_8

A. Honecker¹, F. Meier², Daniel Loss², and B. Normand^{3a}

¹ Institut für Theoretische Physik, TU Braunschweig, Mendelssohnstr. 3, D-38106 Braunschweig, Germany

² Département für Physik und Astronomie, Universität Basel, CH-4056 Basel, Switzerland

³ Theoretische Physik III, Elektronische Korrelationen und Magnetismus, Institut für Physik, Universität Augsburg, D-86135 Augsburg, Germany

Received: Feb. 22nd, 2002

Abstract. We present detailed calculations of low-energy spin dynamics in the “ferric wheel” systems Na:Fe_6 and Cs:Fe_8 in a magnetic field. We compute by exact diagonalisation the low-energy spectra and matrix elements for total-spin and Néel-vector components, and thus the time-dependent correlation functions of these operators. Comparison of our results with the semiclassical theory of coherent quantum tunnelling of the Néel vector demonstrates the validity of a two-state description for the low-energy dynamics of ferric wheels. We discuss the implications of our results for mesoscopic quantum coherent phenomena, and for the experimental techniques to observe them, in molecular magnetic rings.

PACS. 75.10.Jm Quantised spin models – 03.65.Sq Semiclassical theories and applications – 73.40.Gk Tunnelling – 75.30.Gw Magnetic anisotropy

1 Introduction

Quantum coherent tunnelling of the magnetic moment in nanoscopic magnets has recently become the focus of strong experimental and theoretical activity [1]. The ferric wheel systems Fe_N (Fig. 1) present a particularly promising subgroup in which crystals have now been prepared of compounds with $N = 6, 8, 10, 12$ and 18 magnetic Fe(III) ions in ring geometry [2, 3, 4, 5, 6, 7, 8]. These molecules have antiferromagnetic (AF) coupling between spins $s = 5/2$ on each iron site, show a ground state with vanishing total spin $S = 0$ at zero field, and because of an effective uniaxial magnetic anisotropy admit the possibility of mesoscopic quantum phenomena in the form of coherent tunnelling of the Néel vector [9, 10, 11, 12].

The best characterised molecular rings are Fe_{10} [5, 6], various realisations of Fe_6 [2, 3], which differ in ligand group and central alkali metal ion, and Cs:Fe_8 [4]. These materials have been studied by a variety of experimental techniques, including magnetic susceptibility and torque magnetometry [2, 13, 14, 15], specific heat [16], electron spin resonance (ESR) [17], inelastic neutron scattering (INS) [14] and spin relaxation in nuclear magnetic resonance (NMR) [18]. All of these studies serve essentially to characterise the zero-field spectrum and the dependence of the energetic separation of the lowest two levels on the applied field, both of which may be encapsulated within

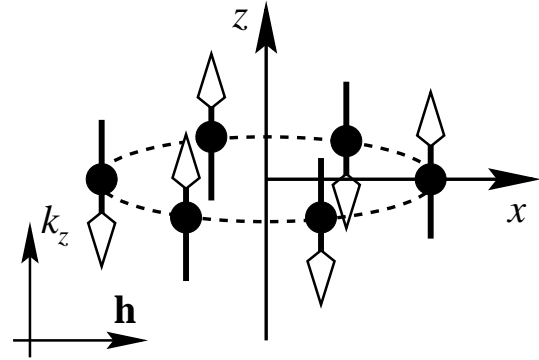


Fig. 1. Schematic representation of an Fe_6 ring with spins aligned along the easy axis (\hat{z}), whose orientation is normal to the ring plane. The field $\mathbf{h} = g\mu_B\mathbf{B}$ is applied in the plane of the ring.

a phenomenological Hamiltonian written in terms of only the total spin [6, 13].

In contrast to the situation in the ferromagnetic (FM) molecular clusters Mn_{12} and Fe_8 [19], the notion of spin quantum tunnelling in the AF ferric wheels has to date received little experimental attention. On the theoretical side, a semiclassical description of the low-energy dynamics provides the clear prediction [12] of coherent tunnelling of the staggered moment. Analysis of magnetisation and torque measurements in this framework [20] allows one to

^a Present address: Département de Physique, Université de Fribourg, CH-1700 Fribourg, Switzerland

extract the AF superexchange J and an effective uniaxial anisotropy k_z for the ring molecules. k_z determines the height of the tunnel barrier between the degenerate energy minima, and thus the extent to which quantum transitions may influence the system response at the lowest temperatures.

Although technical difficulties certainly arise in coupling directly to the staggered moment, the ferric wheels appear to offer significant advantages over FM molecules for the experimental observation of coherent tunnelling. In all such molecular crystals there are many possible sources of decoherence [20] which act to destroy the coherent nature of the predicted tunnelling processes. These we discuss in further detail in Sec. IV. Here we note only that any measurement of quantum coherence effects would require at minimum that the decoherence time Γ^{-1} be significantly longer than the tunnelling time Δ^{-1} . From the semiclassical theory, summarised in Sec. 2, Δ is the level separation in the low-energy (two-state) manifold, and corresponds to the tunnel splitting. In the FM systems $\Gamma \gg \Delta$, and mesoscopic spin quantum tunnelling is said to be incoherent. While the reasonable assumption that decoherence rates, Γ , are not vastly different in the FM and AF systems remains to be proven, the tunnelling frequency, Δ , is some 6-7 orders of magnitude larger in the AF ferric wheels, making these very good candidates for the observation of coherent tunnelling. We note here that none of the above types of experiment offers a means to extract a decoherence rate or to distinguish between coherent and incoherent tunnelling.

The decoherence rate can be determined only from dynamical quantities [21], whose spectral linewidths provide an upper bound on Γ . In the strictest sense, experimental confirmation of the inequality $\Gamma \ll \Delta$ still does not establish the existence of coherent dynamics, an undertaking which would require a true time-domain observation of an appropriate oscillating quantity. In this study we seek to establish that coherent oscillations, including coherent tunnelling processes, are indeed present in the dynamical properties of ferric wheel systems without decoherence. That this is not a trivial statement is clear both phenomenologically from the apparent success of a model requiring only the total spin [6,13], and microscopically from the huge number of states $[(2s+1)^N]$, energy-level splittings and possible matrix elements involved in a complete description. Establishment of the presence and nature of quantum coherence in these mesoscopic molecular systems would provide both an existence proof for coherent spin tunnelling if the condition $\Gamma \ll \Delta$ is satisfied, and valuable guidance for its experimental observation.

Thus we present a detailed investigation of the dynamical properties of the ferric wheels Na:Fe₆ and Cs:Fe₈ by exact diagonalisation (ED). A necessary initial step is to identify those dynamical quantities from which information on the quantum dynamics of interest may be obtained. This task is straightforward for FM molecular clusters, but is less immediately evident in ferric wheels, where, with the exception of a recent examination of electronic and nuclear spin dynamics in a semiclassical frame-

work [21], a full analysis of microscopic dynamical properties is still lacking for the realistic Hamiltonian. The spin dynamics of rings with AF Heisenberg interactions has attracted some recent interest (see Refs. [22,23] and references therein). However, previous studies have been restricted to systems without anisotropy, which are not expected to show mesoscopic quantum phenomena in the form of coherent Néel vector tunneling.

In contrast, we consider here the spin dynamics of a full, effective Hamiltonian for the ferric wheels Fe₆ and Fe₈. The calculation of dynamical quantities, which we obtain from total-spin and Néel-vector correlation functions, then provides essential new information adding to the understanding of the physical properties of ferric wheels. Such a study is required not only to establish the existence of quantum coherent oscillations in a microscopic model for a complex, mesoscopic system, but also to aid the extraction of decoherence rates from experimental dynamical quantities. On the theoretical level, dynamical studies are qualitatively more difficult than the calculation of ground-state properties [20] because they require that excited states and all corresponding matrix elements be taken into account. We note that a very recent, related study [24] of the systems Fe₆ to Fe₁₂, while technically advanced, includes the anisotropy only at the level of a low-energy effective Hamiltonian and does not consider intrinsic dynamical correlations in the presence of a time-independent magnetic field.

The manuscript is organised as follows. In Sec. 2 we present the model Hamiltonian and observables, and provide a brief overview of the technique by which they are analysed. In Sec. 3 we present our results for Na:Fe₆ and Cs:Fe₈, both in the time domain and by analysis of matrix elements, and illustrate their physical origin by comparison with semiclassical approaches. In Sec. 4 we discuss the microscopic understanding of quantum coherence, decoherence sources and the prospects for experimental observation of spin tunnelling in ferric wheels. Sec. 5 contains a summary and conclusions.

2 Model and Method

We work within the minimal model Hamiltonian for AF rings with effective uniaxial anisotropy [12,20,21],

$$H = J \sum_{i=1}^N \mathbf{s}_i \cdot \mathbf{s}_{i+1} - k_z \sum_{i=1}^N s_{i,z}^2 + \mathbf{h} \cdot \sum_{i=1}^N \mathbf{s}_i, \quad (1)$$

where $N = 6$ or 8 , $\mathbf{s}_1 = \mathbf{s}_{N+1}$ and $\mathbf{h} = g\mu_B \mathbf{B}$. J is the superexchange interaction which favours an AF spin configuration on the ring, k_z is the effective uniaxial anisotropy, of dipolar and single-ion origin, and the final term is the Zeeman coupling. In the following all energies and fields are scaled to J and \hbar is set to unity. We define the total-spin operator

$$\mathbf{S} = \sum_i^N \mathbf{s}_i \quad (2)$$

and the Néel-vector operator

$$\mathbf{n} = \frac{1}{N_S} \sum_i^N (-1)^i \mathbf{s}_i. \quad (3)$$

For finite anisotropy the total spin is not a good quantum number, meaning that k_z leads to mixing of different spin multiplets, as will be evident from anticrossings in the energy spectra as a function of field to be shown below. This is a principal reason why numerical calculations are required to make further progress in a quantitative analysis of Eq. (1). The dynamical variables we consider are the autocorrelation functions of the total-spin and Néel-vector operators,

$$\mathcal{S}_{\alpha\alpha}(t) = \langle S_\alpha(t) S_\alpha(0) \rangle \quad (4)$$

and

$$\mathcal{N}_{\alpha\alpha}(t) = \langle n_\alpha(t) n_\alpha(0) \rangle, \quad (5)$$

from which one may seek temporal oscillations characteristic of coherent tunnelling dynamics. Working with correlation functions of total spin and Néel vector is advantageous because it allows one to retain some of the spatial symmetries. This simplifies the computation of matrix elements of \mathbf{S} and \mathbf{n} required in addition to the energy spectra for a full understanding of the dynamics.

The dynamical response of a single spin [21] may also be considered directly. However, we state that all relevant dynamical properties are encoded in the two correlation functions above [Eqs. (4,5)], and show that the single-spin quantities can be deduced from these as follows. We denote by e^{ip} the eigenvalue of the one-site translation operator on the ring, and presume that all low-energy states are contained in the sectors $p = 0$ and $p = \pi$, a fact we will verify below. If the ground state, $|0\rangle$, is in the sector $p = 0$, then matrix elements $\langle i|S_\alpha|0\rangle$ are finite only for states $|i\rangle$ in the sector $p = 0$ and elements $\langle i|n_\alpha|0\rangle$ are finite only for states $|i\rangle$ in the sector $p = \pi$. Because all states considered are invariant under translations by two lattice sites, \mathbf{S} may be substituted by $\frac{1}{2}N(\mathbf{s}_1 + \mathbf{s}_2)$ and \mathbf{n} by $\frac{1}{2s}(\mathbf{s}_1 - \mathbf{s}_2)$. It follows that single-spin correlation functions are given at low frequencies by

$$\langle s_{1\alpha}(t) s_{1\alpha}(0) \rangle \simeq s^2 \mathcal{N}_{\alpha\alpha}(t) + \frac{1}{N^2} \mathcal{S}_{\alpha\alpha}(t), \quad (6)$$

because the cross-correlation functions $\langle n_\alpha(t) S_\alpha(0) \rangle$ vanish due to the opposing symmetries of \mathbf{n} and \mathbf{S} under one-site translation.

Taking as a guide the semiclassical treatment of Ref. [12], a tunnelling scenario is applicable if the ground and first excited states, $|0\rangle$ and $|1\rangle$, are energetically well separated from all other states and form a (weakly) tunnel-split doublet with splitting $\Delta = E_1 - E_0$. Because the states $|0\rangle$ and $|1\rangle$ have opposite behaviour under translation, as defined above, the total-spin matrix element vanishes in this manifold, $\langle 1|\mathbf{S}|0\rangle = 0$, and $\mathcal{S}_{zz}(t)$ has no coherent oscillations with period characteristic of the tunnelling time Δ^{-1} . By contrast, the dynamical properties of the Néel vector are dominated by tunnelling in the lowest manifold, $|\langle 1|n_z|0\rangle| \sim 1$, so that $\mathcal{N}_{zz}(t)$ should

exhibit coherent oscillations with period $2\pi/\Delta$. The quantities \mathcal{S} and \mathcal{N} are measured through the susceptibilities χ_S and χ_N , which are directly related to Eqs. (4,5) by the fluctuation-dissipation theorem. χ_S'' is accessible in ESR or alternating-current (AC) susceptibility measurements, but, because $\chi_S''(\omega \sim \Delta) = 0$ shows no response at the splitting frequency Δ , does not contain any information on tunnelling dynamics [21,25], by which is meant processes in the low-energy sector. χ_N'' is the quantity which, in accordance with semiclassical theory [12, 21], should show oscillatory behaviour due to coherent Néel vector tunnelling. In the weak tunnelling regime, $\chi_N''(\omega \sim \Delta) \simeq \pi\delta(\omega - \Delta) \tanh(\beta\Delta/2)$ has a delta-function peak at Δ [21], but its experimental observation is not straightforward.

A microscopic analysis of Eq. (1) involves many energy levels coupled by potentially large matrix elements of the operators \mathbf{S} and \mathbf{n} arising from the spin interactions. Qualitatively, the system in a transverse magnetic field (Fig. 1) exhibits two degenerate, classical spin configurations (obtained by reflection in the ring plane), between which the semiclassical approach predicts a tunnelling scenario. However, because of the approximations involved in this description, it is not clear that a fully quantum mechanical treatment of the ferric wheel systems would confirm the presence of two low-lying levels sufficiently well separated from all others, or that $\mathcal{N}_{\alpha\alpha}$ would exhibit coherent oscillations dominated by a single frequency for any choice of α or of the applied field. We use the exact correlation functions, meaning the spectra and matrix elements required in their calculation, to resolve this issue.

Magnetisation curves of Heisenberg rings (Eq. (1) with $k_z = 0$) were computed some time ago using Lanczos ED [26], while recent computations of dynamical properties [23] remain very similar in scope. The situation becomes more complicated in the presence of a non-zero single-ion anisotropy, $k_z \neq 0$, and of a magnetic field applied at an arbitrary angle to the \hat{z} -axis. First, in this case the eigenvectors have a non-trivial dependence on the applied field. Second, when S_z is no longer a good quantum number, the loss of the associated symmetries in spin space causes a substantial increase in the dimensions of the Hilbert spaces. With modern computers it is possible to compute ground-state properties by the Lanczos method without exploiting spatial symmetries, at least in the case of Fe₆ [20]. However, as indicated above, dynamical studies require in addition many excited states and the corresponding eigenvectors, although some spatial symmetries remain which simplify this task. The Lanczos method can also be used for this purpose [27], but becomes substantially more involved.

The complete Hilbert spaces for Fe₆ and Fe₈ rings contain $6^6 = 46656$ and $6^8 = 1679616$ states, respectively. For the general case of Eq. (1), there are no symmetries in spin space [28], but the spatial symmetries of one-site translation and reflection at a given site are present. The ground state in a magnetic field is always located either in the sector with $p = 0$ or with $p = \pi$, and has positive parity with respect to reflection at the selected site. These two sec-

tors also contain the lowest excitations. The dimensions of these sectors are 4291 (107331) for $p = 0$ and 4145 (106680) for $p = \pi$ in the case of Fe₆ (Fe₈). Since the Néel vector connects these two subspaces, we work in the sum of the two spaces, which has dimension 8436 (214011), for the computation of matrix elements and correlation functions.

There are several viable methods for the computation of a large number of extremal eigenvalues and -vectors. We have used a combination of simultaneous vector iteration of a large number of vectors with explicit diagonalisation of the Hamiltonian H in the subspace spanned by these vectors during the iteration [29]. For Fe₆ we have computed the lowest 350 eigenvectors and eigenvalues in the symmetry subspace described above. The error caused by this truncation may be estimated in two ways. One is to examine how the results change on varying the number of states retained, and the other is an exact evaluation at $t = 0$ of the correlation functions (4) and (5) for comparison with the results obtained using the truncated spectral representation. On the basis of both methods we estimate that the truncation leads to errors in the temporal correlation functions for Fe₆ on the order of 10^{-6} of the peak values, meaning that the truncation error is undetectable in any of the figures to be shown below for Fe₆, while numerical errors for the individual eigenstates are considerably smaller still. For Fe₈ we have retained the lowest 50 eigenvectors in the combined subspace, and have an estimated truncation error on the order of 10^{-4} of the peak values in the temporal correlation functions. As noted above, all of our results are obtained for zero temperature using the minimal Hamiltonian (1), and thus include no sources of decoherence.

As in Ref. [20] we will focus on magnetic fields applied in the plane of the ring (Fig. 1), the geometry which retains the highest tunnel barrier, with maximal localisation of the Néel vector, at given field. We have also considered field angles out of the plane of the ring, and confirmed that they yield qualitatively similar results at strong fields. This is to be expected because the physical situation remains one in which the spins are largely confined to a planar motion between two potential minima, and also because in our numerical approach the z -inversion symmetry of the transverse-field case is not essential. Here we calculate dynamical quantities [Eqs. (4,5)] exhibiting oscillations in the time domain, and discuss the information they contain concerning mesoscopic quantum coherent phenomena.

3 Results

3.1 Na : Fe₆

We begin with a discussion of the energy spectrum for the physical system Na:Fe₆, for which $k_z/J = 0.0136$ in Eq. (1) [20]. As the applied field is increased, level crossings occur at critical fields B_{cn} between ground states with increasing total spin and alternating quantum numbers $p = 0$ or $p = \pi$. This leads to a magnetisation curve with

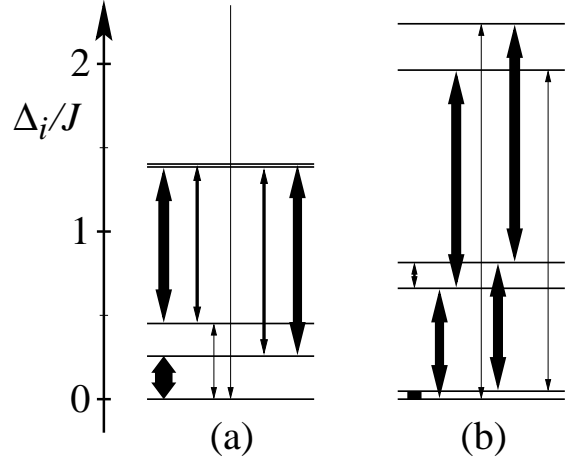


Fig. 2. Lowest energy level spacings $\Delta_i = E_i - E_0$ for an Na:Fe₆ ring described by the minimal Hamiltonian (1), for applied fields $g\mu_B B_x = 3.1J$ (a) and $g\mu_B B_x = 3.5J$ (b). The thickness of the vertical lines represents the magnitude of the matrix elements of n_z connecting each level pair.

an almost regular staircase of plateaux [20]. Guided by the semiclassical prescription that quantum tunnelling is best defined in intermediate fields [12], we consider magnetic fields beyond the lowest magnetisation plateau ($B > B_{c1}$).

Fig. 2 shows the lowest energy levels for two fields chosen near the centre of a magnetisation plateau (a) and very close to a level crossing (b) (see Figs. 5 and 6 below). Near the level crossing, there are indeed two nearly degenerate levels lying well below any of the others, but we stress that this alone is not sufficient to guarantee single-frequency oscillations corresponding to the energy difference Δ in any observable, and thus to justify a two-level tunnelling scenario. This point is represented schematically in Fig. 2 by the lines connecting the levels, the thickness of which corresponds to the magnitude of the matrix element $|\langle i|n_z|j\rangle|$, where i and j denote the energy levels. For fields corresponding to the centre of a plateau, one observes by contrast that there is no clear two-level manifold, but that for certain operators, such as n_z as shown, the matrix element between the lowest pair of levels is dominant. This situation, $|\langle 1|n_z|0\rangle| \sim 1$, can be taken to express the requirement for a two-level description to be adequate for mesoscopic tunnelling of the Néel vector.

3.1.1 Time Domain

There are in principle two ways of testing the coherent low-energy dynamics of a two-level system at low temperatures. The first would be to prepare the system in a non-eigenstate of the Hamiltonian, $|\psi\rangle = (|0\rangle + |1\rangle)/\sqrt{2}$, and then to observe coherent oscillations of the quantity of interest (here n_z) in the time domain. The second is to measure ground-state correlation functions such as $\langle 0|n_z(t)n_z(0)|0\rangle$. For an idealised tunnelling scenario in which n_z connects only $|0\rangle$ and $|1\rangle$, these two quantities

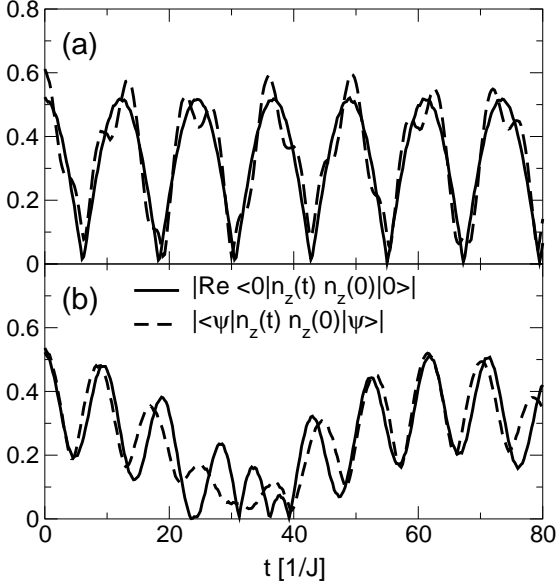


Fig. 3. The Néel vector correlation function $\mathcal{N}_{zz}(t)$ for Na:Fe₆ in magnetic fields (a) $g\mu_B B_x = 3.1J$ and (b) $g\mu_B B_x = 3.5J$.

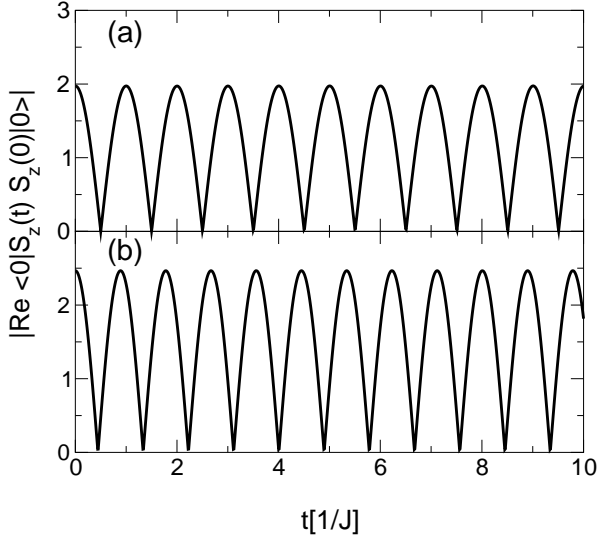


Fig. 4. The total-spin correlation function $\mathcal{S}_{zz}(t)$ for Na:Fe₆ in magnetic fields (a) $g\mu_B B_x = 3.1J$ and (b) $g\mu_B B_x = 3.5J$.

contain the same information because in this case

$$|\text{Re} \langle 0|n_z(t) n_z(0)|0\rangle| \approx |\langle \psi|n_z(t) n_z(0)|\psi\rangle|. \quad (7)$$

In the tunnelling limit, where $|\langle 0|n_z|1\rangle| \sim 1$, one obtains $\langle 0|n_z(t) n_z(0)|0\rangle \simeq |\langle 0|n_z|1\rangle|^2 e^{i\Delta t}$. The correlation functions obtained from ED indeed show coherent oscillations with periods $2\pi/\Delta = 24.5/J$ near the plateau centre [Fig. 3(a)] and $2\pi/\Delta = 132.0/J$ near the level crossing, where in addition a strong component of a higher harmonic is clearly evident [Fig. 3(b)]. The solid and dashed curves in Fig. 3, representing respectively the left- and right-hand sides of the two-level approximation (7), do not coincide

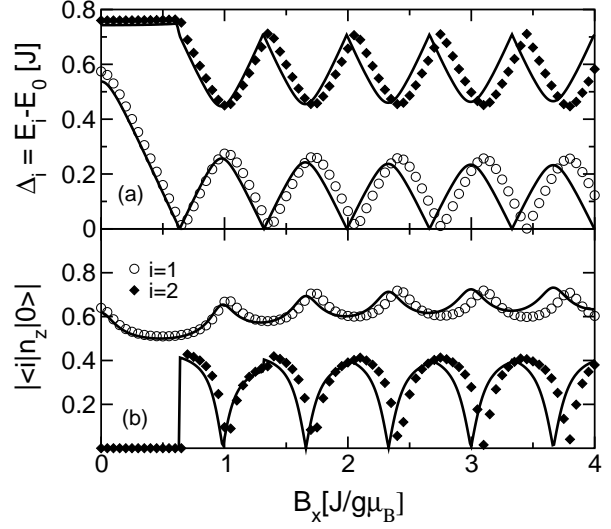


Fig. 5. Evolution with magnetic field of (a) the energy-level splittings Δ_i and (b) the matrix elements $\langle i|n_z|0\rangle$ for the low-energy sector ($i = 1, 2$) in Na:Fe₆. ED results (symbols) are compared with the RR approximation (lines).

because of additional components present in the correlation function of $|\psi\rangle$ [right-hand side of (7)]. These indicate that $|1\rangle$ has significant matrix elements of n_z with states other than $|0\rangle$ (Fig. 2), as a result of which the mapping of Na:Fe₆ onto a two-level system is marginal (below).

In stark contrast to \mathcal{N}_{zz} , the total-spin correlation function \mathcal{S}_{zz} (Fig. 4) shows oscillations only at the much higher frequency $h_x/2\pi$, as expected from the symmetry considerations presented above. While these field-driven oscillations are coherent, they do not correspond to a tunnelling process, where the levels involved lie below the height of the anisotropy barrier, as is the case in the lowest manifold.

3.1.2 Spectra and Matrix Elements

The time-dependent correlation functions shown above may be understood directly from the matrix elements between the lowest-lying energy levels for the components of the total-spin and Néel-vector operators. The symbols in Fig. 5 show the numerical results for energy-level splittings and matrix elements of n_z in the low-energy manifold of Na:Fe₆. The energy separations Δ_i [Fig. 5(a)] confirm that an appreciable separation remains between the lowest pair of states and the next higher level for all fields. That this criterion alone is not sufficient to assess the quality of a two-level description is shown by the matrix elements in Fig. 5(b). While $\langle 1|n_z|0\rangle$ is indeed large for all fields, the matrix element $\langle 2|n_z|0\rangle$ is also significant at fields close to the level crossings. In fact at the plateau centers $\langle 2|n_z|0\rangle$ vanishes identically, and in this field regime $\langle 1|n_z|0\rangle$ is considerably larger than $\langle i|n_z|0\rangle$ for all $i \geq 2$. Our ED calculations confirm that the semiclassical picture of a tunnelling, or coherent oscillation at sub-barrier energies

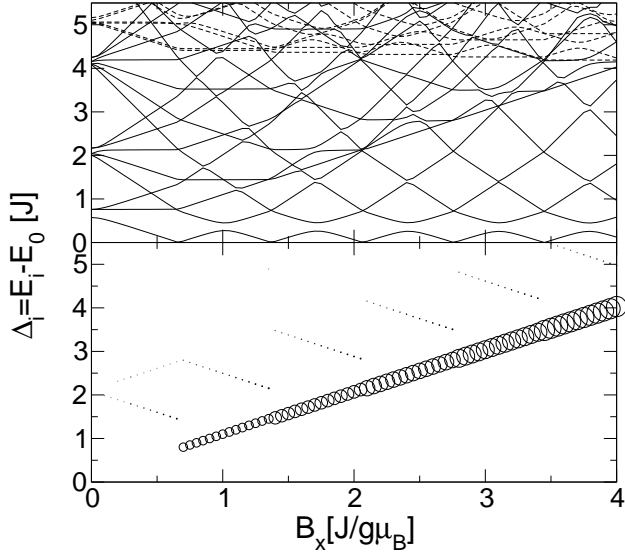


Fig. 6. (a) Evolution with magnetic field of energy spectra for Na:Fe₆ up to $\Delta_i = 5.5J$. The solid lines represent ED data in the momentum sectors $p = 0$ and $p = \pi$ (in both cases, only states with positive site parity appear in the energy range of the figure), while the dashed lines correspond to momenta $p = \pi/3$ and $p = 2\pi/3$ which are absent in the RR model. Note the almost linearly Zeeman-split state at $\Delta_i \approx h_x$. (b) Matrix element $|\langle i|S_z|0\rangle|$ as a function of magnetic field, represented by radius of open circles. The dominant matrix element corresponds to the level with $\Delta_i \approx h_x$ for $h_x \geq 0.7J$, while for the same field range the next-largest elements correspond to still higher excited levels.

of the Néel vector between directions $+\hat{e}_z$ to $-\hat{e}_z$, is indeed appropriate here. By contrast, at the level-crossing fields more of the higher matrix elements of n_z are appreciable [Fig. 2(b)], and in particular $\langle 2|n_z|0\rangle$ has 66.0% of the magnitude of $\langle 1|n_z|0\rangle$. In the semiclassical description this corresponds to the Néel vector being rather less well localised along $\pm\hat{e}_z$ than for fields at the plateau centers. The effects of the higher matrix elements with $|0\rangle$ [Fig. 5(b)] are clear in the difference between the solid lines in Figs. 3(a) and (b), while those of the elements with $|1\rangle$ are visible in the differences between solid and dashed lines in Fig. 3.

Fig. 6(a) shows the spectrum of Na:Fe₆ as a function of field, expanded to splittings $\Delta_i = 5.5J$, which illustrates both the predominance of the anticrossing between the second and third levels and the presence of a linearly evolving Zeeman-split level at $\Delta_i \approx h_x$. The total-spin matrix elements in Fig. 6(b) show the two primary features expected on symmetry grounds: the matrix element in the low-energy sector vanishes, $\langle 1|S_z|0\rangle = 0$, and the dominant matrix element appears at the Zeeman splitting. This situation remains very close to the $k_z = 0$ limit, where the field-driven Zeeman transition is the only process with a non-vanishing matrix element, $|\langle i|S_z|0\rangle| = \sqrt{S(h_x)/2}$, in which $S(h_x)$ denotes the spin of the ground state at field h_x .

To clarify the issue of the importance of choosing n_z and S_z , we comment that we have also studied correlation functions of the other components of \mathbf{n} and \mathbf{S} . These quantities confirm that oscillations generically similar to those observed in \mathcal{N}_{zz} and \mathcal{S}_{zz} remain. However, the correlation functions of the vectors tend to show less clearly defined oscillations as compared to those of the z -components, because the transverse components couple rather more strongly to further levels.

3.1.3 Rigid-Rotor Model

Further insight may be gained into the nature of our exact results by comparison with those from semiclassical approaches [11,12,20], which specify the conditions for the two-level system to provide an appropriate description of the low-energy spectrum of Eq. (1). Under the assumptions that the spins in the ferric wheel have alternating (Néel) alignment and that magnon excitations may be neglected, H can be mapped to the Hamiltonian of a rigid rotor (RR) [12],

$$H_{\text{RR}} = \frac{2J}{N}\mathbf{L}^2 + \mathbf{h} \cdot \mathbf{L} - Nk_z s^2 n_z^2, \quad (8)$$

where \mathbf{n} and \mathbf{L} are respectively the position and angular momentum of a particle confined to the unit sphere. The operator for total spin is represented by the angular momentum of the particle, $\mathbf{S} = \mathbf{L}$, the eigenstates of which, $|l, m\rangle$, are spherical harmonics. The term $-Nk_z s^2 n_z^2$ accounts for the anisotropy potential which renders energetically favourable those spin configurations for which the Néel vector \mathbf{n} is aligned with $\pm\hat{e}_z$. For small k_z , the eigenstates of Eq. (8) have almost uniform probability distribution of \mathbf{n} in the plane perpendicular to the magnetic field, which corresponds to the kinetic limit of H_{RR} . The opposite limit of large k_z is specified by the condition that the tunnel action $\mathcal{S}_0 = Ns\sqrt{2k_z/J}$ be very much greater than 1 [12], and it is here that a two-level description of quantum tunnelling of the staggered magnetisation is appropriate.

The condition $\mathcal{S}_0 > 1$ may be taken to mark the onset of a spin quantum tunnelling regime, in which there is only one pair of tunnel-split states in the low-energy sector. In this respect a two-level approximation is marginal for the real materials, although should be rather better defined for Cs:Fe₈ ($\mathcal{S}_0 = 3.8$) and Fe₁₀ ($\mathcal{S}_0 = 3.3$) than for Na:Fe₆ ($\mathcal{S}_0 = 2.5$). In this regime of intermediate k_z/J the RR framework remains applicable, but the anisotropy energy $-Nk_z s^2 n_z^2$, which may not be treated perturbatively, gives rise to significant mixing of states of differing angular momentum l . A quantitative comparison of RR results with ED then requires exact diagonalisation of Eq. (8). This is most easily performed in the basis $|l, m\rangle$ in which \mathbf{L} is diagonal, and the matrix elements $\langle l', m'|n_z^2|l, m\rangle$ are evaluated in spherical coordinates. For moderate fields, the unphysical states of large angular momenta ($l > 15$) may be neglected in the RR approach, and the dimension of the Hilbert space is then strongly reduced from that of the full Hamiltonian (256 compared to 46656 for Fe₆).

Comparisons between ED of the RR model (8) and the exact numerical results are shown in Fig. 5. There is rather good general agreement in the low-energy sector, especially in magnitudes of Δ_i and $|\langle i|n_z|0\rangle|$, but also a drift in field of the predicted magnetisation step positions from the exact result [30]. This is thought to be largely a consequence of neglecting magnon excitations, by which is meant spin misalignments within each of the sublattices, and can be removed by a uniform rescaling (with a factor of 1.036 for the parameters of Na:Fe₆). The RR model is not expected to perform as well at higher energies, a statement which can be quantified by inspection of the exact spectra shown in Fig. 6(a), where energy levels corresponding to the neglected momentum sectors $p = \pi/3$ and $2\pi/3$ appear at $\Delta_i > 4J$. However, the RR prediction of the total-spin matrix elements shown in Fig. 6(b) remains quite accurate for the energies shown, including the qualitative result that no matrix elements of the total-spin components connect $|0\rangle$ and $|1\rangle$ and the quantitative result for the ground-state spin $S(h_x) \sim \lfloor Nh_x/4J \rfloor$ appearing in the only large matrix element $|\langle i|S_z|0\rangle| \approx \sqrt{S(h_x)}/2$ at $\Delta_i \approx h_x$. We may summarise by remarking that, for $S_0 > 1$, the two-level paradigm [12,21] delivers a simple conceptual picture of the low-energy spin dynamics in terms of coherent tunnelling of the staggered magnetisation, and that in addition the semiclassical treatment based on ED of the RR approximation provides semi-quantitative accuracy for the physical parameters of the real materials.

3.2 Cs : Fe₈

We turn briefly to the 8-membered ferric wheel Cs:Fe₈. The effective uniaxial anisotropy which may be extracted from the magnetisation data for this material [14] is considerably stronger than in the case of Na:Fe₆ presented above. Numerically, dynamical simulations remain possible for this system, despite the much larger Hilbert space. Fig. 7 shows the energy spectrum for a Cs:Fe₈ system, again described by Eq. (1), with the anisotropy ratio deduced [20] from the angle-dependence of the first critical field [14] to be $k_z/J = 0.0185$. The situation remains qualitatively similar to Na:Fe₆, but has visible differences as a result of the larger values of N and k_z/J . The stronger coupling between eigenstates $|l, m\rangle$ results in a stronger anticrossing of levels $|1\rangle$ and $|2\rangle$ at the plateau centers and a smaller maximal Δ . This enhanced separation of the two-state manifold at lowest energies, combined with an increased tunnel barrier, makes the semiclassical tunnelling description more appropriate, as expected from the larger value of S_0 . Although in Fig. 7 we show only the results of full diagonalisation, we have verified that, as in the case of Na:Fe₆, the RR model again provides qualitatively similar results, albeit with a larger drift in the level-crossing fields.

Fig. 8 shows the Néel vector correlation function for the system in two magnetic fields chosen close to a plateau centre and to a plateau edge. We observe rather clean, single-component temporal oscillations near the centre of

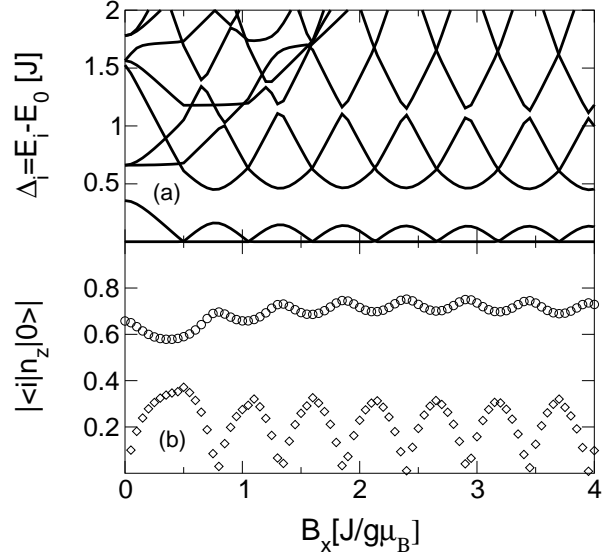


Fig. 7. Evolution with magnetic field of (a) energy-level splittings Δ_i and (b) matrix elements $\langle i|n_z|0\rangle$ for the low-energy sector in Cs:Fe₈. In (b), the circles correspond to $i = 1$ and diamonds to $i \geq 2$.

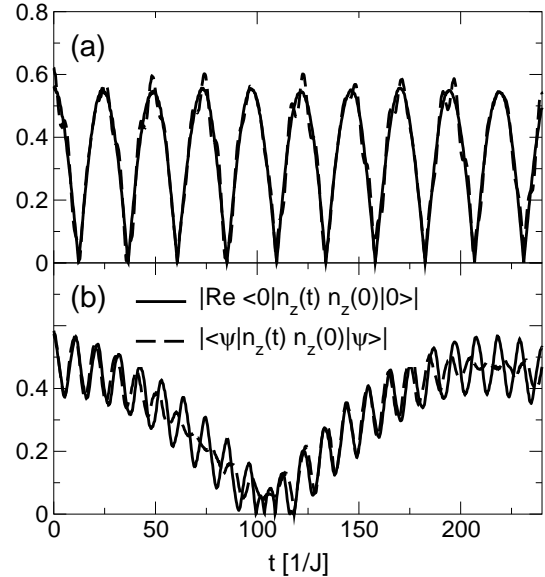


Fig. 8. The Néel vector correlation function $\mathcal{N}_{zz}(t)$ for Cs:Fe₈ in magnetic fields (a) $g\mu_B B_x = 3.4J$ and (b) $g\mu_B B_x = 3.72J$.

the magnetisation plateau [Fig. 8(a)], where the admixture of higher frequencies is indeed weak. Near the level crossing [Fig. 8(b)] the second-largest matrix element, $\langle 2|n_z|0\rangle$, has 43.4% of the magnitude of $\langle 1|n_z|0\rangle$, demonstrating again the reduced validity of the two-level description at these fields, compared to the plateau centers. However, the large separation in frequency scales results in clearly visible contributions from both components, and thus to pronounced low-frequency oscillations in \mathcal{N}_{zz} corresponding to coherent Néel vector tunnelling in Fig. 8(b).

4 Discussion

4.1 Nature of mesoscopic quantum dynamics

With the aid of the two-level analogue we obtain a conceptual picture of the microscopic nature of quantum coherence. The main result of our ED study is that the correlation functions of the total spin and the Néel vector, $\mathcal{S}_{\alpha\alpha}(t)$ and $\mathcal{N}_{\alpha\alpha}(t)$ respectively, show qualitatively different behaviour. Although both exhibit almost single- (or two-)frequency oscillations for the parameters illustrated here, the frequencies of these oscillations are very different. While $\mathcal{S}_{zz}(t)$ oscillates at a frequency determined by the (strong) magnetic field, $\omega = h_x$, $\mathcal{N}_{zz}(t)$ exhibits oscillations with a much smaller frequency, $\omega = \Delta$. The amplitude of the Néel-vector correlation function, $\mathcal{N}_{zz}(t) \lesssim 1$, also allows one to conclude that the oscillations indeed correspond to a true quantum tunnelling. Hence, although most features of the thermodynamic properties and the ESR spectra of ferric wheels can be understood from a phenomenological total-spin Hamiltonian [6,13], their most interesting dynamical feature, quantum coherent spin tunnelling, is not contained in such a description.

The clearest example of spin tunnelling would be obtained by preparing a two-level system in the state $|\psi\rangle$ introduced in Sec. 3.1.1. For a ferric wheel this state would correspond to a spin configuration of the type represented in Fig. 1, with the Néel vector oriented in the direction $+\hat{e}_z$. $|\psi\rangle$ is a superposition of energy eigenstates whose evolution proceeds according to the phase factors e^{-iE_it} of the energy levels, without disturbance by external processes (decoherence), such that after every odd number of half cycles the degenerate state $|\bar{\psi}\rangle = (|0\rangle - |1\rangle)/\sqrt{2}$, corresponding to the Néel vector oriented along $-\hat{e}_z$, is achieved.

In the microscopic analysis of the ferric wheel, we have demonstrated two important features in the realisation of such an idealised tunnelling scenario. First, it is indeed possible to reduce the complex physical system to an effective two-state model, by application of a strong field in the ring plane. In this case, the dominant matrix element of the selected operator n_z is that connecting the two levels in the low-energy manifold, such that \mathcal{N}_{zz} exhibits single-frequency oscillations at the splitting frequency Δ , which corresponds to tunnelling dynamics of the Néel vector. We stress in this connection that single-frequency oscillations depend not only on the energetic separation of the levels involved (from each other or from all others in the spectrum), but essentially on the matrix elements. While other single-frequency oscillations may be found in a dissipationless quantum system, for the ferric wheel only that in the low-energy manifold corresponds to a tunnelling process. The second key feature is that in this situation the difficult experimental step of establishing the non-eigenstate $|\psi\rangle$ is not essential, given a suitable measurement of the equilibrium correlation function $\mathcal{N}_{zz}(t)$. We discuss in Sec. 4.3 below the possibilities for executing this nontrivial task.

Finally, we comment that the ferric wheels are intermediate in size between a minimal quantum system such as two coupled $s = 1$ spins with anisotropy and the classical

limit of a large total (staggered) spin $S \gg 1$ with at least two degenerate minima in an energy continuum. Comparison of our exact numerical results with analytical expressions for small systems, and with the RR model, provides a prescription for understanding the evolution of coherent phenomena with system size, and the accompanying evolution of the appropriate description from microscopic to semiclassical.

4.2 Decoherence

As already discussed in Sec. 1, we have not included decoherence within our numerical calculations. On the technical level this can be effected by the inclusion of a generic bath coupled to the quantum system [31]. However, with the aim of establishing the nature of coherent oscillations in the mesoscopic ferric wheel systems, we have restricted the present discussion to the pragmatic level on which decoherence times Γ^{-1} significantly longer than tunnelling times Δ^{-1} are a prerequisite for any observation of coherent phenomena [1].

In the ferric wheel systems the tunnel splitting frequencies Δ are very large: at the centers of the magnetisation plateaux, where we have shown that the clearest single-frequency oscillations should be present, the tunnel frequencies are $\Delta = 235\text{GHz}$ (11.4K) in Na:Fe₆, 62GHz (3.0K) in Cs:Fe₈ and 45GHz (2.2K) in Fe₁₀. At low temperatures in a sufficiently pure crystal, decoherence will be due primarily to additional interactions not included in the minimal Hamiltonian of Eq. (1). The intrinsic decoherence rate, Γ , for ferric wheels is most likely to be controlled by interring dipolar interactions of electron spins (10-50mK), and possibly by interring superexchange processes, whose contributions are very difficult to estimate but may exceed 0.1K [25]. Nuclear dipolar interactions with ¹H nuclei (0.1mK) and hyperfine interactions with ⁵⁷Fe nuclei (1mK) are sufficiently weak [21] that they may be neglected in these systems. An approximate upper limit for Γ in Na:Fe₆ may be taken from the broadening of the lowest magnetisation step at 40mK [32], which was measured as 0.4T (0.54K), although this is considerably smaller than the broadenings observed at the magnetisation steps by NMR relaxation rate measurements in Li:Fe₆ [33]. In any event, even with these worst-case decoherence estimates, the ferric wheels Fe₁₀, Cs:Fe₈ and Na:Fe₆ remain by the $\Delta \gg \Gamma$ criterion very promising candidates for observation of coherent spin tunnelling.

4.3 Detection of coherent tunnelling

Using the above picture of mesoscopic quantum coherence at the microscopic level, one would like to consider those experiments or techniques which may be applied in order to detect coherent quantum tunnelling in the ferric wheels. Unfortunately, our prescription is at first sight rather exacting, as it requires observing time-dependent correlation functions of the Néel vector. An observation would then depend on a probe coupling to the staggered moment of

the AF rings. The closest available options for dynamical investigations are the local spin-raising and -lowering operations ($\Delta s_i^z = \pm 1$) in NMR and INS studies. We have argued that single-spin dynamics in the ring indeed reflects the Néel vector response, and thus conclude that these techniques are in principle capable of revealing the existence of coherent tunnelling processes at frequency Δ . The matrix elements we have computed could also be used to fit transition intensities higher in the INS spectrum. In contrast to these probes, ESR is sensitive only to the total spin \mathbf{S} of the ferric wheels, and thus, as shown above and in Ref. [21], cannot detect mesoscopic Néel vector tunnelling. The matrix elements for total spin indicate that the ESR response would be dominated by the field-driven Zeeman transition.

However, technical problems arise which would make any observation of quantum coherence very difficult for the pure ferric wheels which are known. NMR measurements suffer from the very weak matrix elements coupling the nuclear spins to the electronic system [21], and from the mismatch in frequency scales between the maximal Δ and the probe frequency. Neutron scattering studies would require a large, deuterated single crystal. Here we suggest only that the most appropriate way forward would be to expand the range of viable experiments by considering rings with a strongly broken symmetry, as may be achieved by doping with nonmagnetic ($s = 0$) impurities [25], such as Ga in ferric wheels. These modified ferric wheels retain the AF properties required to satisfy the condition $\Delta \gg T$, and in addition possess an excess, or tracer, spin which may be followed with a magnetic field. The dynamical properties of these systems are expected to retain the quantum tunnelling characteristics of the undoped systems [25], with the important additional feature that the total spin \mathbf{S} also reflects the coherent tunnelling of \mathbf{n} , which would then become accessible by ESR [21]. We will address in a forthcoming publication the microscopic and experimental aspects of dynamics in modified ferric wheels.

5 Summary

In conclusion, we have presented a numerical and semiclassical analysis of low-energy spin dynamics and quantum coherent tunnelling phenomena in the molecular magnetic ring systems Na:Fe₆ and Cs:Fe₈. The energy-level spectra and the matrix elements for total-spin and Néel-vector operators computed at different magnetic field values establish the presence of quantum coherent oscillations in their correlation functions. Oscillations corresponding to coherent tunnelling of the staggered magnetisation are present for systems with the physical parameters of the ferric wheels, with the cleanest single-frequency, or two-level, oscillations found in the response of the Néel vector at applied fields in the centers of intermediate magnetisation plateaux. These results show that, despite the small system size ($N = 6$ or 8) and small spin quantum number $s = 5/2$, the semiclassical picture of Néel vector tunnelling [12] provides a valid picture of the low-energy dynamical

properties of ferric wheels. Experimental observation of mesoscopic quantum oscillations is possible with probes which flip local electronic spins, and would appear to be most feasible in studies of broken-symmetry systems obtainable by doping of the ring materials.

Acknowledgements

FM and DL are supported by the Swiss National Fund, Molnanomag HPRN-CT-1999-00012 and BBW Bern. BN is supported by SFB 484 of the Deutsche Forschungsgemeinschaft.

References

1. *Quantum Tunneling of Magnetization*, edited by L. Gunther, B. Barbara (Kluwer, Dordrecht, 1995).
2. A. Caneschi, A. Cornia, A. C. Fabretti, S. Foner, D. Gatteschi, R. Grandi, L. Schenetti, *Chem. Eur. J.* **2**, 1379 (1996).
3. A. Cornia, M. Affronte, A. G. M. Jansen, G. L. Abbati, D. Gatteschi, *Angew. Chem. Int. Ed. Engl.* **38**, 2264 (1999).
4. R. W. Saalfrank, I. Bernt, E. Uller, F. Hampel, *Angew. Chem. Int. Ed. Engl.* **36**, 2482 (1997).
5. D. Gatteschi, A. Caneschi, L. Pardi, R. Sessoli, *Science* **265**, 1054 (1994).
6. K. L. Taft, C. D. Delfs, G. C. Papefthymiou, S. Foner, D. Gatteschi, S. J. Lippard, *J. Am. Chem. Soc.* **116**, 823 (1994).
7. A. Caneschi, A. Cornia, A. C. Fabretti, D. Gatteschi, *Angew. Chem. Int. Ed. Engl.* **38**, 1295 (1999).
8. S. P. Watton, P. Fuhrman, L. E. Pence, A. Caneschi, A. Cornia, G. L. Abbati, S. J. Lippard, *Angew. Chem. Int. Ed. Engl.* **36**, 2774 (1997).
9. B. Barbara, E. M. Chudnovsky, *Phys. Lett. A* **145**, 205 (1990).
10. I. V. Krive, O. B. Zaslavskii, *J. Phys. Cond. Matt.* **2**, 9457 (1990).
11. D. Loss, D. P. DiVincenzo, G. Grinstein, *Phys. Rev. Lett.* **69**, 3232 (1992).
12. A. Chiolero, D. Loss, *Phys. Rev. Lett.* **80**, 169 (1998).
13. A. Cornia, A. G. M. Jansen, M. Affronte, *Phys. Rev. B* **60**, 12177 (1999).
14. O. Waldmann, J. Schülein, R. Koch, P. Müller, I. Bernt, R. W. Saalfrank, H. P. Andres, H. U. Güdel, P. Allenspach, *Inorg. Chem.* **38**, 5879 (1999).
15. O. Waldmann, R. Koch, S. Schromm, J. Schülein, P. Müller, I. Bernt, R. W. Saalfrank, F. Hampel, E. Balthes, *Inorg. Chem.* **40**, 2986 (2001).
16. M. Affronte, J. C. Lasjaunias, A. Cornia, A. Caneschi, *Phys. Rev. B* **60**, 1161 (1999).
17. B. Pilawa, R. Desquiotz, M. T. Kelemen, M. Weickenmeier, A. Geisselmann, *J. Magn. Mag. Mater.* **177-181**, 748 (1998).
18. M.-H. Julien, Z. H. Jang, A. Lascialfari, F. Borsa, M. Horvatić, A. Caneschi, D. Gatteschi, *Phys. Rev. Lett.* **83**, 227 (1999).
19. see W. Wernsdorfer, R. Sessoli, *Science* **284**, 133 (1999), and references therein; M. N. Leuenberger, D. Loss, *Phys. Rev. B* **61**, 1286 (2000), and references therein.

20. B. Normand, X. Wang, X. Zotos, D. Loss, Phys. Rev. B **63**, 184409 (2001).
21. F. Meier, D. Loss, Phys. Rev. Lett. **86**, 5373 (2001).
22. R. Werner, A. Klümper, Phys. Rev. B **64**, 174414 (2001).
23. O. Waldmann, Phys. Rev. B **65**, 024424 (2002).
24. I. Rudra, S. Ramasesha, D. Sen, cond-mat/0201330 (unpublished).
25. F. Meier, D. Loss, Phys. Rev. B **64**, 224411 (2001).
26. J. B. Parkinson, J. C. Bonner, Phys. Rev. B **32**, 4703 (1985).
27. J. K. Cullum, R. A. Willoughby, *Lanczos Algorithms for Large Symmetric Eigenvalue Computations, Vol. I* (Birkhäuser, Boston, 1985).
28. For a field in the x - y plane, z -direction spin inversion is a further symmetry, which we have, however, not exploited.
29. A version of the programme which we have used may be downloaded from <http://www.tu-bs.de/~honecker/software/diagonalize.html>.
30. J. Schnack, M. Luban, Phys. Rev. B **63**, 014418 (2001).
31. see K. Saito, S. Miyashita, H. De Raedt, Phys. Rev. B **60**, 14553 (1999), and references therein.
32. A. Cornia, A. G. M. Jansen, M. Affronte, unpublished.
33. A. Lascialfari *et al.*, unpublished.